



Cosmic microwave background measurements can discriminate among inflation models

Scott Dodelson*

*NASA/Fermilab Astrophysics Center
Fermi National Accelerator Laboratory, Batavia, IL 60510*

William H. Kinney†

*NASA/Fermilab Astrophysics Center
Fermi National Accelerator Laboratory, Batavia, IL 60510*

Edward W. Kolb‡

*NASA/Fermilab Astrophysics Center
Fermi National Accelerator Laboratory, Batavia, IL 60510, and
Department of Astronomy and Astrophysics, Enrico Fermi Institute
The University of Chicago, Chicago, IL 60637*

Quantum fluctuations during inflation may be responsible for temperature anisotropies in the cosmic microwave background (CMB). Observations of CMB anisotropies can be used to falsify many currently popular models. In this paper we discuss the prospectus for observations of CMB anisotropies at the accuracy of planned satellite missions to reject currently popular inflation models and to provide some direction for model building.

PACS number(s): 98.80.Cq, 98.80.Es, 98.70.Vc

*Electronic mail: dodelson@hermes.fnal.gov

†Electronic mail: kinneyw@fnal.gov

‡Electronic mail: rocky@rigoletto.fnal.gov



I. INTRODUCTION

The field of observational cosmology has developed to the degree that it is now possible to test models of the early universe. The next few years should see a dramatic increase in the variety and accuracy of cosmological observations. In this paper, we discuss how measurements of the temperature anisotropies in the cosmic microwave background (CMB) at the accuracy expected to result from two planned satellite missions, the Microwave Anisotropy Probe (MAP) [1] and PLANCK (formerly COBRAS/SAMBA) [2], will allow us to discriminate among inflation models.

The basic idea of inflation is that there was an epoch early in the history of the universe when potential, or vacuum, energy dominated other forms of energy density such as matter or radiation. During the vacuum-dominated era the scale factor grew quasi-exponentially while the Hubble radius remained roughly constant. Since in cosmic expansion length scales increase with the scale factor, scales that were once smaller than the Hubble radius grew during inflation to become larger than the Hubble radius. Once a length scale becomes larger than the Hubble radius, any perturbation on that scale becomes frozen. Once inflation ends and the universe is radiation or matter dominated, the Hubble radius increases faster than the scale factor and the length scale reenters the Hubble radius with the signature of events during inflation imprinted upon it.

By observing fluctuations in the CMB or fluctuations in the distribution of matter, we can observe the signature of quantum fluctuations during inflation. Since different potentials lead to different signatures, we can see which inflation models are consistent with CMB fluctuations¹. A problem with this effort [7,8] of trying to extract information about the inflaton potential from the CMB is that the anisotropies depend not only on

¹We are assuming that inflation is responsible for the anisotropies. There has recently been a large amount of work [3,4,5,6] trying to understand how easy it will be to distinguish anisotropies produced by inflation from those produced by other mechanisms. We do not enter into this debate here.

the inflationary parameters, but also on a variety of other unknown cosmological parameters [9,10,11]. Among these are the baryon density Ω_B , the Hubble constant H_0 , and the cosmological constant Λ . Here, we fix the cosmological constant to zero. Allowing Λ and/or other parameters to vary would loosen the constraints on inflationary models. On the other hand, we have not included information that will be gained from measurements of CMB polarization or from ongoing ground-based and balloon measurements of temperature anisotropies. So we expect our final constraints to be realistic indicators of what we will know in ten years.

II. INFLATION DYNAMICS AND CMB FLUCTUATIONS

In this paper we consider only inflation models with “normal” gravity (i.e., general relativity) and a single scalar field (the *inflaton*). Although this might seem like a small region in the space of possible inflation models, it does include some of the most studied models, including scalar field models with polynomial potentials (ϕ^n), pseudo Nambu-Goldstone potentials (natural inflation), exponential potentials (dilaton-like models), or Coleman-Weinberg potentials (“new” inflation). In Section IV we will describe the individual models we test.

In addition to the models we study, many other types of inflation models can be studied by considering an equivalent one-field, slow-roll model. Two familiar examples are the Starobinski R^2 model and versions of extended inflation. Both these models have non-minimal gravitational sectors, with an R^2 term in the action of the Starobinski model, and a Brans-Dicke coupling of R to a scalar field in extended inflation. Although at first sight these do not appear to be included in the class of models we study, after a suitable conformal transformation both models can be expressed as single-field, slow-roll

inflation models. It would be interesting to see if models with more than one inflaton field can be similarly rewritten in terms of a single effective field. However, we do not pursue this possibility here.

A. Perturbation amplitudes and spectral indices from inflation

Our goal is to start with a scalar field potential and calculate the scalar and tensor perturbation amplitudes and spectral indices. We make three basic approximations. The first approximation is a dual expansion of the metric about a Friedmann–Robertson–Walker background, $g_{\mu\nu}(\mathbf{x}, t) = g_{\mu\nu}^{\text{FRW}}(t) + h_{\mu\nu}(\mathbf{x}, t)$, and an expansion of the inflaton field about a homogeneous, isotropic background, $\phi(\mathbf{x}, t) = \phi_0(t) + \delta\phi(\mathbf{x}, t)$. Since we know that the density perturbations are of order 10^{-5} , this is presumably a very good approximation.

The metric perturbations produced by inflation can be described in terms of two functions, which we call $A_S(k)$ and $A_T(k)$. The first function, $A_S(k)$, describes *scalar* metric perturbations. These are the perturbations that couple to $T_{\mu\nu}$ and are associated with structure formation. The second function, $A_T(k)$, describes *tensor* perturbations. The tensor perturbations do not couple to $T_{\mu\nu}$ and are not associated with structure formation. The tensor perturbations can be visualized as gravity waves. The distribution of cosmic radiation depends on the full structure of the metric, so both $A_S(k)$ and $A_T(k)$ contribute to CMB anisotropies.

The perturbation amplitudes $A_S(k)$ and $A_T(k)$ are the values the quantities have when the wavenumber k is equal to the Hubble radius after inflation. The scalar amplitude is related to the density perturbation $(\delta\rho/\rho)_k$ and the power spectrum, $P_S(k) \propto k^{-3}(\delta\rho/\rho)_k^2$, through a transfer function $T(k)$ [12]. We note that the normalization of A_S and A_T is somewhat arbitrary, although the choice of normalization will affect how we relate the

parameters to directly observable quantities; we follow the convention of Ref. [13]. There $A_S(k)$ is normalized to be equal to the density perturbation at Hubble radius crossing: $A_S(k = aH) = (\delta\rho/\rho)_{k=aH}$. The normalization of $A_T(k)$ was chosen such that to lowest order $A_T^2 = \epsilon A_S^2$, where ϵ is defined below.

The favored formalism for the calculation of perturbations uses the Hamilton-Jacobi formulation of scalar field dynamics during inflation [14,15,16], where the expansion rate, H , parameterized by the value of the scalar field, ϕ , is viewed as the fundamental dynamical variable. The most accurate calculations of the perturbation spectra are in terms of H and its derivatives. The derivatives of H can be expressed in terms of dimensionless *slow-roll parameters*, the first two of which are defined as²

$$\epsilon(\phi) \equiv \frac{m_{Pl}^2}{4\pi} \left(\frac{H'(\phi)}{H(\phi)} \right)^2; \quad \eta(\phi) \equiv \frac{m_{Pl}^2}{4\pi} \frac{H''(\phi)}{H(\phi)}. \quad (2.1)$$

The second approximation we make involves the assumption that the slow-roll parameters are small in comparison to unity. Note that ϵ is a direct measure of the equation of state of the scalar field matter, $p = -\rho(1 - 2\epsilon/3)$, where p is the pressure and ρ is the energy density. Since inflation can be defined to be a period of accelerated expansion, where

$$\left(\frac{\ddot{a}}{a} \right) = H^2(1 - \epsilon) > 0, \quad (2.2)$$

the end of inflation can be expressed exactly as $\epsilon = 1$.

In the Hamiltonian-Jacobi formulation of the dynamics, the expansion rate $H(\phi)$ is the fundamental cosmological parameter. However, in comparison with particle physics models, the inflaton potential $V(\phi)$ is fundamental. Thus, we have to express the slow-roll parameters in terms of the inflaton potential. This was done in Ref. [17], with result

$$\epsilon(\phi) = \frac{m_{Pl}^2}{16\pi} \left(\frac{V'(\phi)}{V(\phi)} \right)^2; \quad \eta(\phi) = -\frac{m_{Pl}^2}{16\pi} \left(\frac{V'(\phi)}{V(\phi)} \right)^2 + \frac{m_{Pl}^2}{8\pi} \left(\frac{V''(\phi)}{V(\phi)} \right). \quad (2.3)$$

²The definition of the slow-roll parameters vary; we follow the conventions of Ref. [13].

The value of the scalar field can be used to specify a length scale crossing the Hubble radius during inflation. This is most easily accomplished by considering the number of e-foldings of the scale factor in the evolution from a value of ϕ until the end of inflation:

$$N(\phi, \phi_{\text{END}}) \equiv \int_t^{t_{\text{END}}} H(t) dt = \pm \frac{4\pi}{m_{\text{Pl}}^2} \int_{\phi}^{\phi_{\text{END}}} \frac{H(\phi)}{H'(\phi)} d\phi, \quad (2.4)$$

where the subscript ‘END’ signifies that the quantity is to be evaluated at the end of inflation. The choice of sign depends upon the sign of $\dot{\phi}$, i.e., whether $|\phi_{\text{END}}|$ is greater or less than $|\phi|$. It can be fixed by requiring the right-hand side of the equation to be positive.

The comoving scale k crosses the Hubble radius during inflation $N(k)$ e-foldings from the end of inflation, where $N(k)$ is given by [13]

$$N(k) = 62 - \ln \frac{k}{a_0 H_0} - \ln \frac{10^{16} \text{GeV}}{V_k^{1/4}} + \ln \frac{V_k^{1/4}}{V_e^{1/4}} - \frac{1}{3} \ln \frac{V_e^{1/4}}{\rho_{\text{RH}}^{1/4}}. \quad (2.5)$$

The subscript ‘0’ indicates the present value of the quantity and ρ_{RH} is the energy density after reheating. For instance, a length scale corresponding to $200h^{-1}$ Mpc (i.e., $k = 2\pi/200h^{-1}\text{Mpc}$) roughly corresponds to $N(\phi, \phi_e) \simeq 50$. Therefore the value of the inflaton field when a comoving scale of $200h^{-1}$ Mpc crosses the Hubble radius during inflation is found by finding ϕ_{END} and solving Eq. (2.4) with $N(\phi, \phi_{\text{END}}) = 50$.

To lowest order in the slow-roll parameters, the scalar and tensor perturbation spectra are

$$A_S(k) \simeq \frac{2}{5\sqrt{\pi}} \frac{1}{\sqrt{\epsilon(\phi)}} \frac{H(\phi)}{m_{\text{Pl}}}; \quad A_T(k) \simeq \frac{2}{5\sqrt{\pi}} \frac{H(\phi)}{m_{\text{Pl}}}. \quad (2.6)$$

Note that the left hand side is expressed in terms of wavenumber k . The relationship between ϕ and k was discussed above.

It is useful to describe the spectra in terms of spectral indices $n \equiv d \ln A_S^2(k)/d \ln k$ and $n_T \equiv d \ln A_T^2(k)/d \ln k$. Again to lowest order in the slow-roll parameters,

$$n(k) - 1 \simeq -4\epsilon(\phi) + 2\eta(\phi), \quad n_T(k) \simeq -2\epsilon(\phi), \quad (2.7)$$

where once again it is necessary to use the relationship between k and ϕ . A third approximation we make is that over the range of length scales probed by CMB we can take the spectral indices as *constant*. In other words we assume that although the slow-roll parameters change in inflation, they are roughly constant during the epoch where scales of interest for the CMB cross the Hubble radius. This implies that the scalar and tensor spectra can be written as

$$A_S(k) = A_S(k_0) \left(\frac{k}{k_0}\right)^{1-n} ; \quad A_T(k) = A_T(k_0) \left(\frac{k}{k_0}\right)^{n_T} , \quad (2.8)$$

where n and n_T are *constant* and k_0 is the wavenumber corresponding to some length scale probed by CMB experiments. This allows the two *functions*, $A_S(k)$ and $A_T(k)$, to be parameterized in terms of four *constants*, $\{A_S(k_0), A_T(k_0), n, n_T\}$.

If the perturbations arise from slow-roll inflation, then not all of the four parameters are independent, but there is a relation, known as the *consistency relation*, which reduces the number to three. To lowest order in slow-roll parameters, the consistency relation can be found from Eqs. (2.6) and (2.7): $n_T = -2A_T(k_0)^2/A_S(k_0)^2$. So within the framework of the approximations discussed above, the scalar and tensor perturbation spectra can be characterized by three parameters, $\{A_S(k_0), A_T(k_0), n\}$.

B. Parameterization of the CMB perturbation spectrum

To calculate CMB spectra, one must solve the perturbed Einstein-Boltzmann equations which describe how the different components of the universe (photons, neutrinos, electrons, protons, hydrogen, and dark matter) couple to each other and to gravity. The perturbation spectra produced by inflation are taken as initial conditions for these equations. The final output is the full spectrum of CMB perturbations. In Gaussian theories, such as inflation, these are completely characterized by the two-point correlation function.

If the temperature pattern on the sky is expanded in spherical harmonics,

$$\frac{\delta T(\theta, \phi)}{T_0} = \sum_{l=0}^{\infty} \sum_{m=-l}^l a_{lm} Y_{lm}(\theta, \phi) \quad (2.9)$$

where $T_0 = 2.726$ is the average temperature of the CMB today, then inflation predicts that each a_{lm} will be Gaussian distributed with mean zero and variance

$$C_l \equiv \langle |a_{lm}|^2 \rangle. \quad (2.10)$$

The C_l 's can be both measured experimentally and predicted theoretically.

For a given set of inflationary parameters and cosmological parameters, one can determine the full spectrum of C_l 's by solving the Einstein-Boltzmann equations. Therefore, instead of specifying thousands of C_l 's, it is more convenient to characterize a given spectrum by the parameters which determine it. These are the three parameters of the initial perturbation spectra, $\{A_S(k_0), A_T(k_0), n\}$ plus the unknown cosmological parameters, which we take to be Ω_B and H_0 . It has become conventional to re-express the amplitudes $A_S(k_0)$ and $A_T(k_0)$ in terms of two more physical quantities related to C_2 . Specifically, we introduce two parameters

$$Q_{rms-PS} \equiv T_0 \sqrt{\frac{5C_2}{4\pi}} \quad \text{and} \quad r \equiv \frac{C_2^{\text{tensor}}}{C_2^{\text{scalar}}}. \quad (2.11)$$

Thus, any given set of C_l 's that we consider is a function of five parameters, which we take to be Q_{rms-PS} , r , n , Ω_B , and H_0 .

C. Connecting slow-roll parameters and CMB parameters

The natural parameters in ‘‘model space’’ are H , ϵ , and η , which correspond to the expansion rate during inflation, and the first and second derivative of the expansion rate. Since most inflation models have an arbitrary adjustable parameter corresponding to the normalization, information on the magnitude of H is not as valuable as information about

the way H changes. (Equivalently, no theory predicts the value of Q_{rms-PS} .) So we find that information about ϵ and η gleaned from the harvest of information expected from the next generation of CMB satellites will be the best discriminant of inflation models. Here we relate ϵ and η to the observationally relevant parameters n and r .

Equation 2.7 can be used to relate n to ϵ and η . The only ambiguity is the value of ϕ at which to evaluate ϵ and η . The most reasonable value of ϕ is the one which corresponds to scales probed by the CMB. Thus, we define ϕ_{CMB} to be the value of ϕ associated with $N(\phi_{\text{CMB}}, \phi_{\text{END}}) = 50$. (This is sometimes called ϕ_{50} or ϕ_* .) By using Eq. (2.4), ϕ_{CMB} is found from

$$N(\phi_{\text{CMB}}, \phi_{\text{END}}) = 50 = \sqrt{\frac{4\pi}{m_{Pl}^2}} \int_{\phi_{\text{CMB}}}^{\phi_{\text{END}}} \frac{1}{\sqrt{\epsilon(\phi')}} d\phi' . \quad (2.12)$$

Then n is given by

$$n = 1 - 4\epsilon_{\text{CMB}} + 2\eta_{\text{CMB}} \quad (2.13)$$

where $\epsilon_{\text{CMB}} \equiv \epsilon(\phi_{\text{CMB}})$ and similarly for η .

While the tensor to scalar ratio r depends on $A_T(k_0)/A_S(k_0)$, it also depends on n somewhat, since C_2 coming from both tensors and scalars is actually an integral over the primordial spectra. Using fits to these integrals provided in Ref. [18], it is straightforward to show that, to lowest order in slow-roll,

$$r = 13.7\epsilon_{\text{CMB}}. \quad (2.14)$$

We now have all the ingredients for a recipe to compare inflation model predictions to CMB information. The steps are:

1. From $V(\phi)$, calculate $\epsilon(\phi)$ and $\eta(\phi)$ using Eq. (2.3).
2. Calculate ϕ_{END} by $\epsilon(\phi_{\text{END}}) = 1$.

3. Find ϕ_{CMB} using Eq. (2.12).
4. From ϵ_{CMB} and η_{CMB} calculate n from Eq. (2.13) and r from Eq. (2.14), which can be compared directly to CMB temperature anisotropy data.

III. SOME ONE-FIELD, SLOW-ROLL INFLATION MODELS

In this section, we look at several generic inflationary models. The models we consider can be grouped into three general classes, “large-field,” “small-field,” and “hybrid.” Large-field models are characterized by so-called *chaotic* initial conditions, in which the inflaton field is displaced far from its minimum, typically to values $\phi \sim m_{\text{Pl}}$, and rolls toward a minimum at the origin. Examples A and E below are large-field models. Small-field models are of the form that would be expected as a result of spontaneous symmetry breaking, with a field initially near the origin and rolling toward a minimum at $\langle\phi\rangle \neq 0$. In this case, inflation occurs when the field is small relative to its expectation value, $\phi \ll \langle\phi\rangle$. Examples B and C below are small-field models.

In order to avoid cumbersome notation we will assume that ϕ is positive. Clearly if the potential is an even function of ϕ then the sign of ϕ is irrelevant, while if the potential is an odd function of ϕ , then $-V(-\phi)$ is equivalent to $V(\phi)$.

The large-field and small-field cases occupy very different regions in the space of observable parameters, and can be formally distinguished by the curvature of the potential in the region where inflation is taking place: for the large field models, $V''(\phi) > 0$, and for the small field models, $V''(\phi) < 0$. In addition, we consider a fifth model (D) that sits on the boundary between the small field and large field cases, which is the case of a linear potential $V''(\phi) = 0$.

A third general class of models, occupying a distinct region of parameter space, is “hybrid” inflation [19,20,21], which is characterized by a field evolving toward a minimum of the potential with a nonzero vacuum energy. Hybrid models generally involve more than one scalar field, but can be treated during the inflationary epoch as single-field inflation, with ϕ small and $V''(\phi) > 0$. Hybrid inflation is the only class of models which predicts a “blue” spectrum, $n > 1$. Case F below is a generic hybrid model.

The idea is to be as general as possible, and we calculate the values of observables as functions of parameters in the models avoiding prejudices about the “reasonableness” of those parameters. For example, it is possible that particular realizations of these cases in more detailed contexts may require excessive fine-tuning or implausibly large mass scales. However, a completely different model may achieve the same behavior in a more natural way, and our goal is inclusiveness. This results in particularly broad constraints in the hybrid case. Hybrid inflation models as a class have enough adjustable parameters that it is possible to generate observables covering broad regions on the (r, n) plane, and model-dependent physical arguments must be invoked to limit the predictions. Nonetheless, even with very weak assumptions, there is no overlap in parameter space between hybrid inflation and the other cases considered.

A. “Large-field” polynomial potentials: $\Lambda^4(\phi/\mu)^p$, $p > 1$

The simplest example of the type of inflation model we study is a “large-field” polynomial potential, $V(\phi) = \Lambda^4(\phi/\mu)^p$ with $p > 1$. Here Λ and μ are parameters of mass dimension one; neither one enters in our results. This potential is often used in “chaotic” inflationary models where some region of the universe starts with the scalar field displaced from the minimum of the potential ($\phi = 0$) by a large amount, typically several times m_{Pl} , and evolves to the minimum. In these models $\phi > \phi_{\text{END}}$, so inflation occurs

when the scalar field is larger than its eventual minimum.

Following the steps outlined in Section II, we find:

1. The slow-roll parameters $\epsilon(\phi)$ and $\eta(\phi)$ are given by

$$\epsilon(\phi) = \frac{p^2}{16\pi} \frac{m_{Pl}^2}{\phi^2}; \quad \eta(\phi) = \frac{p(p-2)}{16\pi} \frac{m_{Pl}^2}{\phi^2} .$$

2. The end of inflation occurs when $\phi = \phi_{\text{END}}$, given by

$$\frac{\phi_{\text{END}}^2}{m_{Pl}^2} = \frac{p^2}{16\pi} .$$

3. The value of ϕ crossing the Hubble radius 50 e-folds from the end of inflation is

$$\frac{\phi_{\text{CMB}}^2}{m_{Pl}^2} = \frac{1}{16\pi} p(p+200) .$$

4. The values of ϵ_{CMB} and η_{CMB} are

$$\epsilon_{\text{CMB}} = \frac{p}{p+200} ; \quad \eta_{\text{CMB}} = \frac{p-2}{p+200} .$$

Using these values of ϵ_{CMB} and η_{CMB} , it is easily shown that

$$n = 1 - \frac{2p+4}{p+200} ; \quad r \simeq 13.7 \frac{p}{p+200} .$$

Note that this is a minimalist model in the sense that inflation ends naturally, without the necessity of invoking another sector of the theory. The results are listed in Table 1.

B. “Small-field” polynomial potentials: $\Lambda^4[1 - (\phi/\mu)^p]$, $\phi \ll \mu \ll m_{Pl}$ and $p > 2$

The small-field polynomial describes what might result if the potential arises from a phase transition associated with spontaneous symmetry breaking. In this scenario, the field is evolving away from an unstable equilibrium at the origin toward a nonzero

vacuum expectation value, $\langle\phi\rangle \neq 0$. Near the origin, the potential can be written as a Taylor expansion,

$$V(\phi) = \Lambda^4 \left[1 - \left(\frac{\phi}{\mu} \right)^p + \dots \right], \quad (3.1)$$

where p is the lowest non-vanishing derivative at the origin, and $\mu \propto \langle\phi\rangle$. For instance, the Coleman-Weinberg potential used in the original “new” inflation models [22,23] is of this form with $n = 4$. This ansatz is quite general, applicable even to potentials which have a logarithmic divergence in the leading derivative at the origin [24]. In keeping with the motivation for this model we will assume that $\mu \ll m_{Pl}$, so we have the hierarchy of scales $\phi \ll \mu \ll m_{Pl}$. The analysis was described in detail in [24]; the relevant results are given in Table 1 and illustrated in Fig. 1. (The case $p = 2$ is special, and is discussed separately below.) Like the polynomial large-field models, the parameters r and n are independent of the fundamental mass scales in the potential,

$$r \simeq 0, \quad n = 1 - \frac{p-1}{25(p-2)}. \quad (3.2)$$

Unlike the large-field case, these models have the feature that ϵ_{CMB} , and hence r , is negligibly small.

C. “Small-field” quadratic potentials: $\Lambda^4[1 - (\phi/\mu)^2]$, $\phi \ll \mu$

“Natural” inflation models [25], in which the potential is usually assumed to have a cosine potential, can be described by Eq. (3.1) with $p = 2$ near the origin where inflation occurs.

Potentials dominated by a quadratic term have the property that the small-field assumption $\phi \ll \mu$, while valid at the time when observable parameters are generated, is

not consistent all the way to the end of inflation, since

$$\epsilon(\phi) = \frac{1}{4\pi} \left(\frac{m_{Pl}}{\mu} \right)^2 \frac{(\phi/\mu)^2}{[1 - (\phi/\mu)^2]^2}. \quad (3.1)$$

Then ϕ_{END}/μ approaches unity for large μ , and higher order terms in the potential cannot be neglected. We adopt the reasonable assumption that μ in some direct sense parameterizes the expectation value of the field in the physical vacuum, so that (ϕ_{END}/μ) is of order unity. The precise value of ϕ_{END} is not important, since

$$\phi_{\text{CMB}} = \phi_{\text{END}} \exp \left[-\frac{25}{4\pi} \left(\frac{m_{Pl}}{\mu} \right)^2 \right] \quad (3.2)$$

is exponentially small regardless, and the parameters ϵ_{CMB} and η_{CMB} approach the small-field limits

$$\eta_{\text{CMB}} = -\frac{1}{4\pi} \left(\frac{m_{Pl}}{\mu} \right)^2, \quad \epsilon_{\text{CMB}} = |\eta_{\text{CMB}}| \exp[-100 |\eta_{\text{CMB}}|] \simeq 0. \quad (3.3)$$

Note that since

$$n = 1 + 2\eta = 1 - \frac{1}{2\pi} \left(\frac{m_{Pl}}{\mu} \right)^2, \quad (3.4)$$

if $n > 0.9$ as suggested by the COBE measurements, then $\mu \ll m_{Pl}$ is excluded. The scale-invariant limit is $\mu \rightarrow \infty$, or $\eta \rightarrow 0$, but it is important to remember that the small-field approximation breaks down in this limit, since $\phi_{\text{CMB}} \rightarrow \phi_{\text{END}}$ in Eq. (3.2).

D. Linear potentials: $\Lambda^4(\phi/\mu)$ and $\Lambda^4[1 - \phi/\mu]$

Linear potentials have the property that $\epsilon = -\eta = m_{Pl}^2/16\pi\mu^2$ is *independent* of ϕ . Thus, if inflation starts, i.e., if $\epsilon < 1$, it will never end. More exactly, some other physics must enter to terminate the inflationary phase. So we assume that the linear potential is only valid when scales of interest for the CMB are passing through the Hubble radius.

Thus the relevant values of ϵ and η are those given above. Like the quadratic potential, the scale-invariant limit is $\mu \rightarrow \infty$.

E. Exponential potentials: $\Lambda^4 \exp \sqrt{16\pi\phi^2/pm_{Pl}^2}$, $p > 0$

Exponential potentials lead to an exponential form of the Hubble parameter, which in turn leads to a power-law time dependence of the scale factor. For potentials of the form $V(\phi) = \Lambda^4 \exp \sqrt{16\pi\phi^2/pm_{Pl}^2}$, the expansion rate is $H \propto \exp \sqrt{4\pi\phi^2/pm_{Pl}^2}$ which gives $a \propto t^p$. This model is usually called power-law inflation, a term we will not use in order to avoid confusion with models with power-law potentials. Exponential potentials, while nonrenormalizable, arise quite naturally as the effective low-energy description of degrees of freedom associated with extra spatial dimensions in Kaluza–Klein models, as well as dilatons and moduli fields in superstring theories.

This model has the useful property that both ϵ and η are constant and equal: $\epsilon = \eta = p^{-1}$. Thus, as in the linear potential case, some other physics must enter in order for inflation to end. With $\epsilon = \eta = p^{-1}$, we find $r = 13.7p^{-1}$ and $n = 1 - 2p^{-1}$. The result $n - 1 \propto r$ is often incorrectly generalized to all slow-roll models.

F. Hybrid Inflation: $\Lambda^4[1 + (\phi/\mu)^p]$, $\phi < \mu$

The final class of models we consider is “hybrid” inflation [19,20,21], in which the field rolls toward a minimum with a nonzero vacuum energy. We take a potential of the form

$$V(\phi) = \Lambda^4 \left[1 + \left(\frac{\phi}{\mu} \right)^p \right], \quad (3.1)$$

with $p \geq 2$. The large-field limit of this potential is just the case of chaotic inflation with a polynomial potential, model A. Hybrid inflation is the limit of *small* field, $\phi < \mu$,

where the potential is dominated by the constant term, $V \simeq \Lambda^4 = \text{const}$. In the absence of any other physics, the field rolls toward the origin, coming to rest at $\phi = 0$ after an *infinite* period of inflation. For inflation to end, another sector of the theory must be invoked, generally a coupling to a second scalar field ψ , so that ϕ_{END} and ϕ_{CMB} cannot be fixed outside the context of a particular model. A generic characteristic, however, is that $\phi_{\text{CMB}} \gg \phi_{\text{END}}$. For generality, we will take (ϕ_{CMB}/μ) to be less than unity; in many models it is often very much less than unity. In hybrid inflation, the parameter η_{CMB} is positive, and can be written in terms of ϵ_{CMB}

$$\begin{aligned} \frac{\eta_{\text{CMB}}}{\epsilon_{\text{CMB}}} &= \frac{2(p-1)}{p} \left(\frac{\phi_{\text{CMB}}}{\mu} \right)^{-p} \left[1 + \frac{p-2}{2(p-1)} \left(\frac{\phi_{\text{CMB}}}{\mu} \right)^p \right] \\ &\longrightarrow \begin{cases} \frac{p-2}{p} & \text{for } \phi_{\text{CMB}}/\mu \gg 1 \\ \frac{2(p-1)}{p} \left(\frac{\mu}{\phi_{\text{CMB}}} \right)^p & \text{for } \phi_{\text{CMB}}/\mu \ll 1 \end{cases} . \end{aligned} \quad (3.2)$$

This first expression depends only on the assumption of slow-roll, not on a small-field limit. In the large-field limit, $\phi_{\text{CMB}}/\mu \gg 1$, we recover the result for model A found above, $\eta_{\text{CMB}}/\epsilon_{\text{CMB}} = (p-2)/p$. In the small-field limit, $\phi_{\text{CMB}}/\mu \ll 1$, we obtain the familiar result for hybrid models, $n > 1$.

This possibility of a “blue” scalar spectrum (here, blue implies $n > 1$) is the distinctive feature of hybrid models. Recalling that $n = 1 - 4\epsilon + 2\eta$, we see that although hybrid models can in principle result in a red spectrum (for $\eta < 2\epsilon$), if $\eta > 2\epsilon$, hybrid inflation predicts a blue spectrum.

The predictions for all of the models described here are summarized in Table 1.

model	$\frac{\phi_{\text{END}}^2}{m_{Pl}^2}$	$\frac{\phi_{\text{CMB}}^2}{m_{Pl}^2}$	ϵ_{CMB}	η_{CMB}
A	$\frac{p^2}{16\pi}$	$\frac{p(p+200)}{16\pi}$	$\frac{p}{p+200}$	$\frac{p-2}{p+200}$
B	$\frac{\mu^2}{m_{Pl}^2} \left[\frac{\sqrt{16\pi}}{p} \left(\frac{\mu}{m_{Pl}} \right) \right]^{2/(p-1)}$	$\frac{\mu^2}{m_{Pl}^2} \left[\frac{4\pi}{25p(p-2)} \left(\frac{\mu^2}{m_{Pl}^2} \right) \right]^{2/(p-2)}$	$\ll \eta_{\text{CMB}} $	$-\frac{p-1}{50(p-2)}$
C	$O\left(\frac{\mu^2}{m_{Pl}^2}\right)$	$\left(\frac{\phi_{\text{END}}^2}{m_{Pl}^2}\right) \exp\left[-\frac{25}{2\pi} \left(\frac{m_{Pl}}{\mu}\right)^2\right]$	$\ll \eta_{\text{CMB}} $	$-\frac{m_{Pl}^2}{4\pi\mu^2}$
D	undetermined	undetermined	$\frac{m_{Pl}^2}{16\pi\mu^2}$	$-\frac{m_{Pl}^2}{16\pi\mu^2}$
E	undetermined	undetermined	p^{-1}	p^{-1}
F	undetermined	undetermined	$< \eta_{\text{CMB}}$	> 0

Table 1: Lowest-order results for ϕ_{END} , ϕ_{CMB} , ϵ_{CMB} , and η_{CMB} in some popular inflation models.

IV. EXTRACTING PERTURBATION SPECTRA INFORMATION FROM CMB OBSERVATIONS

Now that we know how to extract the observables n and r from a given inflationary potential, we turn to the question of how well experiments will be able to measure these quantities. The general question of parameter estimation from CMB experiments will likely occupy cosmologists for a long time. However, without any simulations at all, one can get a very good idea of how accurately parameters will be determined by using a

simple χ^2 technique. A given experiment will measure each C_l with an error given by ΔC_l . The “true” set of parameters will be determined by minimizing

$$\chi^2(\{\lambda_i\}) \equiv \sum_{l=2}^{\infty} \frac{(C_l(\{\lambda_i\}) - C_l^{\text{measured}})^2}{(\Delta C_l)^2}. \quad (4.1)$$

Here the set of parameters $\{n, r, Q_{\text{rms-PS}}, \Omega_B, H_0\}$ which we are allowing to vary is denoted $\{\lambda_i\}$.

Of course, we cannot know in advance what C_l^{measured} will turn out to be. But knowing what we expect for ΔC_l , we can get an estimate of how large the uncertainties in the parameters will be. To do this, we assume that the measured C_l 's will be very close to the true C_l 's. Then, by minimizing the χ^2 , we will accurately determine the parameters. Therefore, we can expand

$$\chi^2(\{\lambda_i\}) \simeq \chi^2(\{\lambda_i^{\text{true}}\}) + \frac{1}{2} \left. \frac{\partial^2 \chi^2}{\partial \lambda_i \partial \lambda_j} \right|_{\lambda=\lambda^{\text{true}}} (\lambda_i - \lambda_i^{\text{true}}) (\lambda_j - \lambda_j^{\text{true}}). \quad (4.2)$$

The second derivative matrix carries information about how quickly the χ^2 increases as the parameters move away from their true values. Therefore, under some reasonable assumptions [26], the uncertainties in the parameters are determined by this matrix. We will be interested only in the parameters n and r , so we want to project these uncertainties onto the two-dimensional $n - r$ plane. (This is equivalent to integrating out all the other variables.) It is a simple exercise to show that these uncertainties are obtained by computing the elements of the five-by-five second derivative matrix, inverting it, and then picking out the two-by-two matrix corresponding to the n, r elements. The remaining two-by-two matrix defines the error ellipses in the $n - r$ plane.

To complete this program, we need two more pieces of information. First, the elements of the derivative matrix must be evaluated at the true values of the parameters. We need to specify what we are assuming for the true values. Here, we look separately at two possible sets of values for the parameters. The first corresponds to standard cold dark

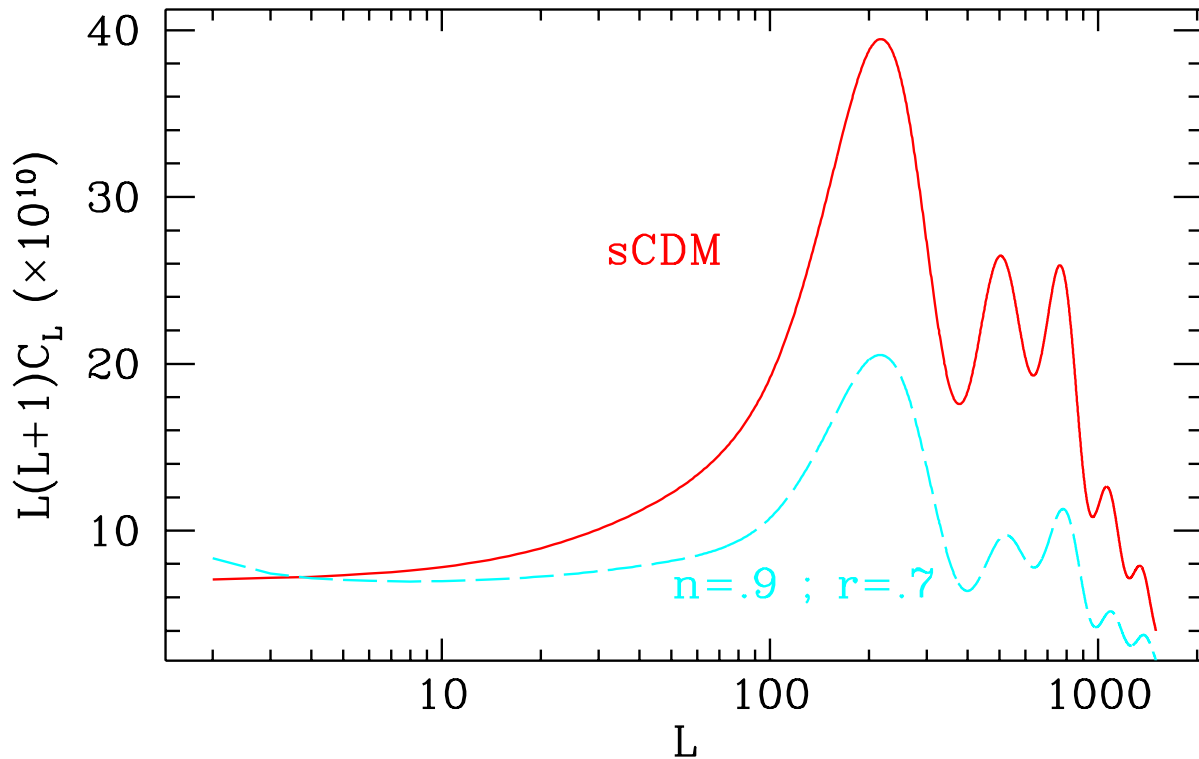


Fig. 1: The spectrum of anisotropies for the two models discussed in the text. Both are normalized at large scales to COBE. The model with $n = 0.9$ is a much better fit to large scale structure data.

matter (sCDM).

$$\{\lambda^{sCDM}\} = \{n, r, Q_{\text{rms-PS}}, \Omega_B, H_0\} = \{1, 0, 18\mu K, 0.0125, 50\} \quad (4.3)$$

where H_0 is in units of $\text{km sec}^{-1} \text{Mpc}^{-1}$. The second set corresponds to values of the parameters considered to be viable upon consideration of large scale structure data [27].

$$\{\lambda^{LSS}\} = \{n, r, Q_{\text{rms-PS}}, \Omega_B, H_0\} = \{0.9, 0.7, 18\mu K, 0.02, 50\} \quad (4.4)$$

The C_l 's for these models are shown in Fig. 1. Since the anisotropies are considerably larger in sCDM, the signal to noise in a given experiment will also be larger. Therefore we expect tighter bounds in sCDM than in our second model.

The last piece of information we need to compute the derivative matrix in Eq. (4.2) is the uncertainty expected in the C_l 's. The relevant experimental parameters are: the

beam width, σ_{beam} ; the expected noise per pixel, σ_{pixel} ; the area per pixel, Ω_{pixel} ; and the fraction of the sky covered. Once these are known, it is very useful to employ a formula derived by Knox [7], who showed that for an all-sky map,

$$\frac{\Delta C_l}{C_l} = \sqrt{\frac{2}{2l+1}} \left(1 + \frac{\sigma_{\text{pixel}}^2 \Omega_{\text{pixel}}}{C_l} \exp\{l^2 \sigma_{\text{beam}}^2\} \right). \quad (4.5)$$

The first term here is the inevitable consequence of the fact that we have only $2l+1$ pieces of information at each l (cosmic variance). We will consider the MAP and PLANCK satellites. For MAP, we assume $\sigma_{\text{beam}} = 0.425 \times 0.3^\circ$ and $\sigma_{\text{pixel}}^2 \Omega_{\text{pixel}} = (35\mu\text{K})^2 (0.3^\circ)^2$. For PLANCK, we take $\sigma_{\text{beam}} = 0.425 \times 0.17^\circ$ and $\sigma_{\text{pixel}}^2 \Omega_{\text{pixel}} = (3\mu\text{K})^2 (0.167^\circ)^2$.

The results are shown in Fig. 2. The ellipses delineate 95% confidence limits in n and r for the sCDM and LSS examples. In the sCDM case, we have imposed the (physical) restriction that $r > 0$. Also shown in Fig. 2 are the predictions from the various models discussed in Section III. By inverting Eqs. (2.13,2.14), we can plot the same ellipses in the $\eta - \epsilon$ plane. These are shown in Fig. 3. The superposition of the ellipses on top of the model predictions makes clear that CMB observations will be able to discriminate amongst inflationary models.

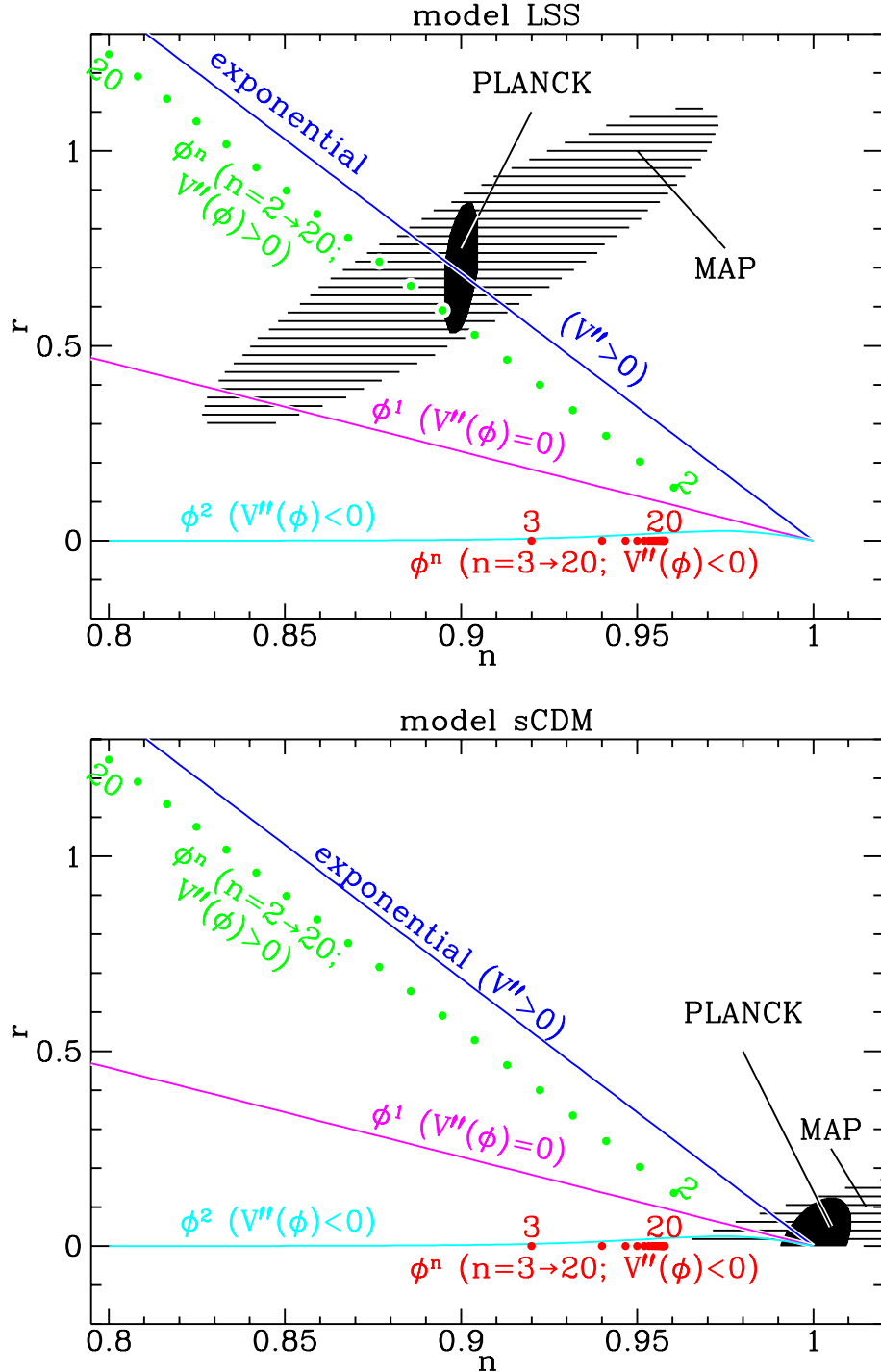


Fig. 2: Predictions for a variety of inflationary models in the $n - r$ plane superimposed on the expected (95% C.L.) region allowed by the two CMB satellites. The two panels correspond to two different values of the true parameters: the upper figure is the LSS model while the lower one is the sCDM model. The line labelled ϕ^1 delineates two classes of models: Large (small) field models lie above (below) the line.

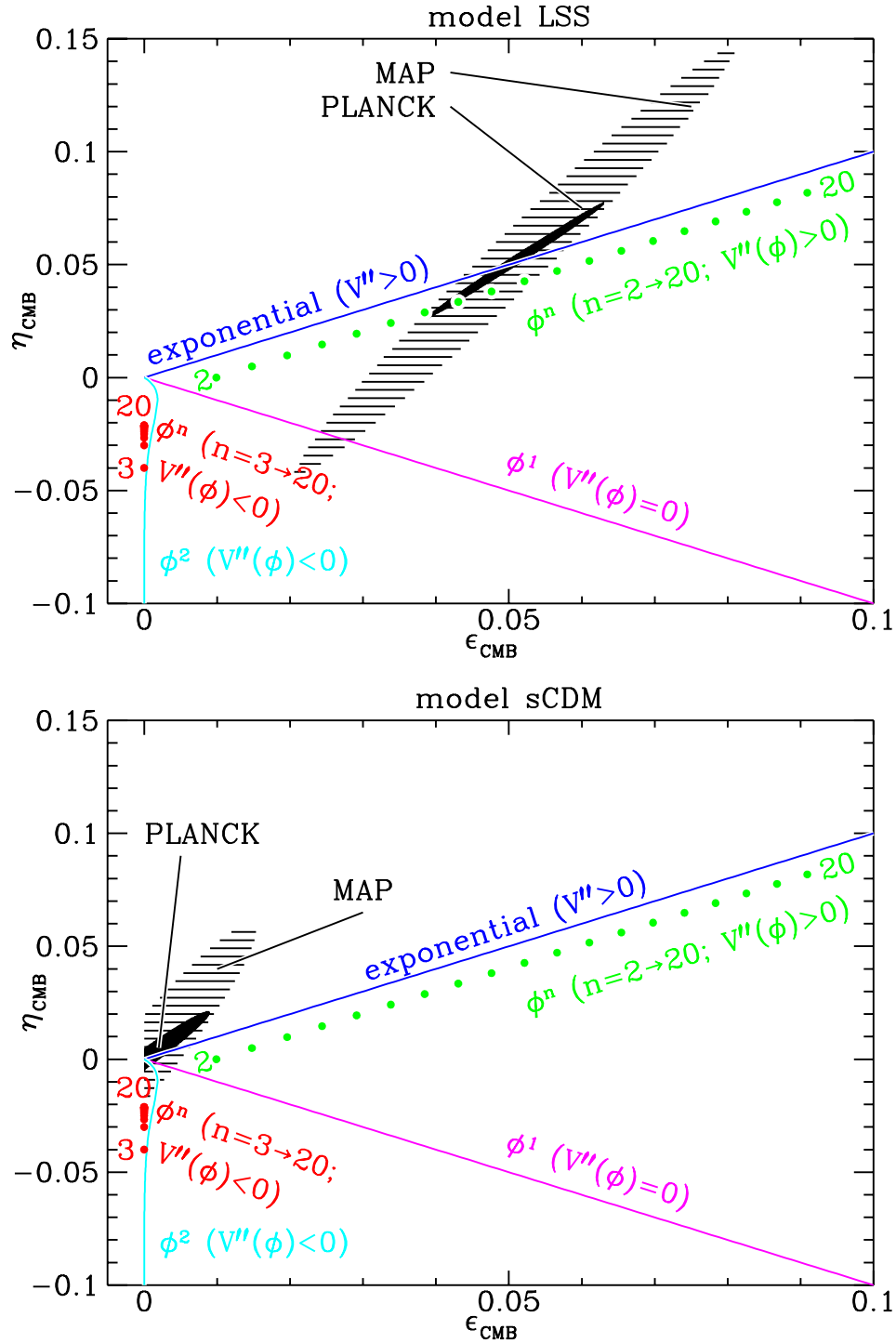


Fig. 3: Same as Fig. 2, but now the observational constraints have been mapped directly onto the $\epsilon - \eta$ plane.

V. CONCLUSIONS

Different inflationary models make different predictions for the spectrum of scalar and tensor perturbations. While very different models might lead to indistinguishable scalar spectra, it has been realized for some time that the tensor spectrum, used in conjunction with the scalar spectrum, can differentiate between models [28]. Here we have demonstrated how the effect of scalar and tensor combinations on CMB fluctuations can be used as a discriminant in testing inflation models.

Most inflationary models have an adjustable parameter that can be tuned to give the correct normalization of the scalar perturbations ($Q_{\text{rms-PS}}$ in the language used to study CMB fluctuations). A simple example of such a parameter is the coupling constant λ in the chaotic inflation model with potential $V(\phi) = \lambda\phi^4$. However, in this paper we have shown that even with the freedom of an adjustable parameter it is possible that observations of the cosmic microwave background can distinguish among different inflation models. Therefore, we can hope in the next decade to see a real confrontation between inflation models and CMB observations.

While the type of analysis we propose can never “prove” that any particular model is correct, it might do much more than simply eliminate models. It is possible that an analysis like the one we present here might be able to give some guidance in model building. One way of dividing inflationary models is to classify them as either “small-field” models, “large-field” models, or “hybrid” models.³ Different versions of the three types of models predict qualitatively different scalar and tensor spectra, so it should be particularly easy to tell them apart once the data is available.

Although we have only studied simple examples of models, we can speculate that small-field, large-field, and hybrid models will populate different regions of the n - r plane

³A more exact division would be according to the second derivative of the potential near ϕ_{CMB} .

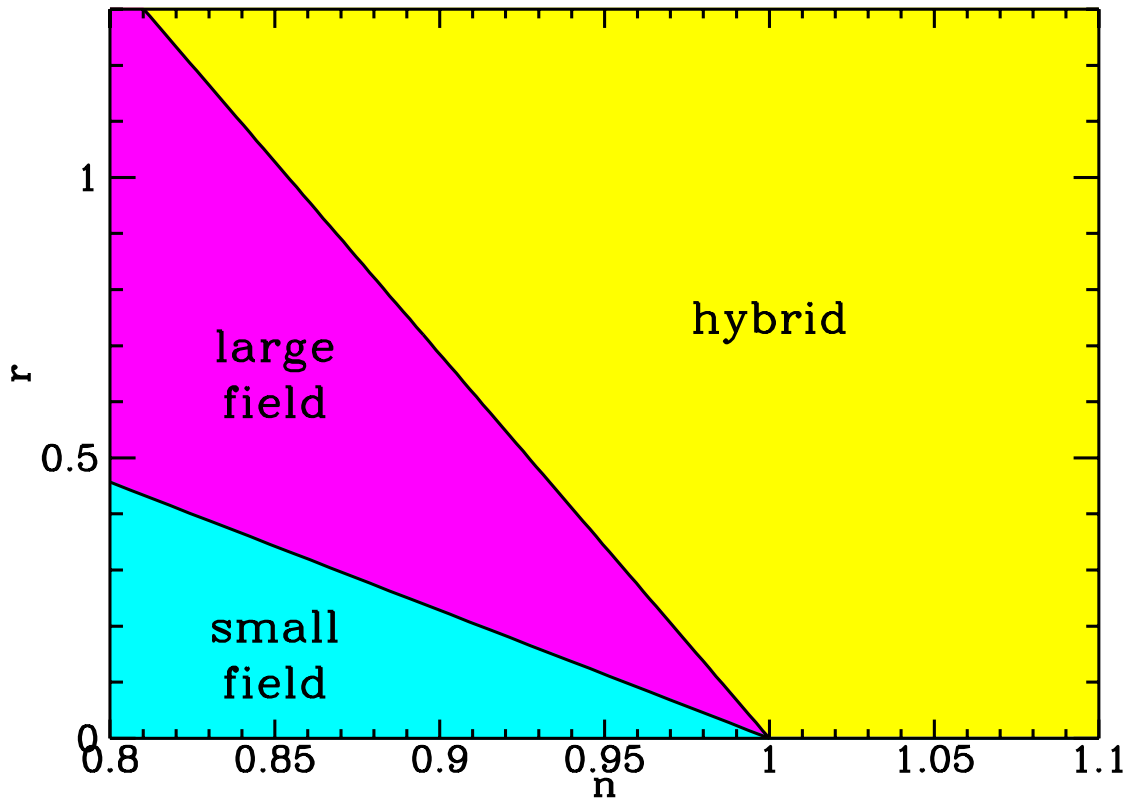


Fig. 4: Regions in the n - r plane populated by the three types of models considered in this paper.

as illustrated in Fig. 4. Certainly a scalar spectral index larger than unity would suggest some form of hybrid model. A scalar index smaller than one in combination with negligible tensor contribution (small r) would suggest a small-field model, while scalar index less than unity with considerable tensor contribution would point toward large-field models.

An interesting question we do not address here is whether single-field, slow-roll models populate the entire n - r plane.

We thank Uros Seljak and Matias Zaldariagga for use of their CMBFAST code [29]. This work was supported in part by DOE and NASA grant NAG5-2788 at Fermilab.

-
- [1] <http://map.gsfc.nasa.gov/>
- [2] <http://astro.estec.esa.nl/SA-general/Projects/Cobras/cobras.html>
- [3] R. G. Crittenden and N. G. Turok, *Phys. Rev. Lett.* **75**, 2642 (1995).
- [4] A. Albrecht, D. Coulson, P. Ferreira, and J. Magueijo, *Phys. Rev. Lett.* **76**, 1413 (1996).
- [5] W. Hu and M. White, *Phys. Rev. Lett.* **77**, 1687 (1996)
- [6] N. G. Turok, astro-ph/9607109 (1996).
- [7] L. Knox, *Phys. Rev. D* **52**, 4307 (1995).
- [8] L. Knox and M. S. Turner, *Phys. Rev. Lett.* **73**, 3347 (1994).
- [9] J. R. Bond, R. Crittenden, R. L. Davis, G. Efstathiou and P. J. Steinhardt, *Phys. Rev. Lett.* **72**, 13 (1994).
- [10] G. Jungman, M. Kamionkowski, A. Kosowsky, D. N. Spergel *Phys. Rev. D* **54**, 1332 (1996).
- [11] S. Dodelson, E. I. Gates, and A. S. Stebbins, *Astrophys. J.* **467**, 10 (1996).
- [12] See, e.g. G. Efstathiou in *Physics of the Early Universe*, edited by J. A. Peacock, A. F. Heavens, and A. T. Davies (Adam Higler, Bristol, 1990).
- [13] J. E. Lidsey, A. R. Liddle, E. W. Kolb, E. J. Copeland, T. Barriero, and M. Abney, *Rev. Mod. Phys.*, (1997).

- [14] L. P. Grishchuk and Yu. V. Sidorav, in *Fourth Seminar on Quantum Gravity*, eds M. A. Markov, V. A. Berezin and V. P. Frolov (World Scientific, Singapore, 1988)
- [15] A. G. Muslimov, *Class. Quant. Grav.* **7**, 231 (1990).
- [16] D. S. Salopek and J. R. Bond, *Phys. Rev. D* **42**, 3936 (1990).
- [17] E. W. Kolb and S. L. Vadas, *Phys. Rev. D*, **50**, 2479 (1994).
- [18] M. S. Turner, M. White and J. E. Lidsey, *Phys. Rev. D* **48**, 4613 (1993).
- [19] A. D. Linde, *Phys. Lett.* **259B**, 38 (1991).
- [20] A. D. Linde, *Phys. Rev. D.* **49**, 748 (1994).
- [21] E. J. Copeland, A. R. Liddle, D. H. Lyth, E. D. Stewart and D. Wands, *Phys. Rev. D* **49** 6410 (1994).
- [22] A. D. Linde, *Phys. Lett.* **108B**, 389 (1982).
- [23] A. Albrecht and P. J. Steinhardt, *Phys. Rev. Lett.* **48**, 1220 (1982).
- [24] W. H. Kinney and K. T. Mahanthappa, *Phys. Rev. D* **53**, 5455 (1996).
- [25] K. Freese, J. Frieman, and A. Olinto, *Phys. Rev. Lett.* **65**, 3233 (1990).
- [26] W. H. Press, S. A. Teukolsky, W. T. Vetterling, and B. P. Flannery, *Numerical Recipes*, (Cambridge: Cambridge University Press, 1992).
- [27] M. White, D. Scott, J. Silk, M. Davis, *Mon. Not. Roy. Astron. Soc.* **276**, L69 (1995).
- [28] E. Copeland, E. W. Kolb, A. R. Liddle, and J. E. Lidsey, *Phys. Rev. Lett.* **71**, 219 (1993) and *Phys. Rev. D* **48**, 2529 (1993).
- [29] U. Seljak and M. Zaldariagga, *Astrophys. J.* **469**, 7 (1996).